

# Holes' character and bond versus charge disproportionation in $s$ - $p$ $ABX_3$ perovskites

Mohammad Reza Benam,<sup>1,2,\*</sup> Kateryna Foyevtsova,<sup>1,2,†</sup> Arash Khazraie,<sup>1,2</sup> Ilya Elfimov,<sup>1,2</sup> and George A. Sawatzky<sup>1,2</sup>

<sup>1</sup>*Department of Physics & Astronomy, University of British Columbia, Vancouver, British Columbia, Canada V6T 1Z1*  
<sup>2</sup>*Stewart Blusson Quantum Matter Institute, University of British Columbia, Vancouver, British Columbia, Canada V6T 1Z4*

We use density functional theory methods to study the electronic structures of a series of  $s$ - $p$  cubic perovskites  $ABX_3$ : the experimentally available  $\text{SrBiO}_3$ ,  $\text{BaBiO}_3$ ,  $\text{BaSbO}_3$ ,  $\text{CsTiF}_3$ , and  $\text{CsTlCl}_3$ , as well as the hypothetical  $\text{MgPO}_3$ ,  $\text{CaAsO}_3$ ,  $\text{SrSbO}_3$ , and  $\text{RaMnO}_3$ . We use tight-binding modeling to calculate the interatomic hopping integrals  $t_{sp\sigma}$  between the  $B$ - $s$  and  $X$ - $p$  atomic orbitals and charge-transfer energies  $\Delta$ , which are the two most important parameters that determine the low-energy electron and hole states of these systems. Our calculations elucidate several trends in  $t_{sp\sigma}$  and  $\Delta$  as one moves across the periodic table, such as the relativistic energy lowering of the  $B$ - $s$  orbital in heavy  $B$  cations leading to strongly negative  $\Delta$  values. Our results are discussed in connection with the general phase diagram for  $s$ - $p$  cubic perovskites proposed in Ref. 26, where the parent superconductors  $\text{SrBiO}_3$  and  $\text{BaBiO}_3$  are found to be in the regime of negative  $\Delta$  and large  $t_{sp\sigma}$ . Here, we explore this further and search for new materials with similar parameters, which could lead to the discovery of new superconductors. Also, some considerations are offered regarding a possible relation between the physical properties of a given  $s$ - $p$  compound (such as its tendency to bond disproportionate and the maximal achievable superconducting transition temperature) and its electronic structure.

PACS numbers:

## I. INTRODUCTION

Materials with a cubic perovskite structure  $ABX_3$ , where the anion  $X$  can be an oxygen or a halogen and the possible cations  $A$  and  $B$  include a broad variety of elements or even molecules, have attracted considerable attention due to their rich physics. Indeed, among their intriguing properties are metal-insulator transitions<sup>1,2</sup>, high transition temperature ( $T_c$ ) superconductivity<sup>3-5</sup>, ferroelectricity, ferromagnetism, applicability in photovoltaics<sup>6</sup>, colossal magnetoresistance<sup>7</sup>, magnetoelectricity<sup>8</sup>, and a topological insulating state<sup>9-11</sup>. The crystal structure of the  $ABX_3$  cubic perovskites consists of a three-dimensional network of corner-sharing  $BX_6$  octahedra intercalated with  $A$  cations at the twelve-fold anion-coordinated sites. One of the well-known and widely studied  $ABX_3$  compounds is  $\text{ABiO}_3$ , with  $A = \text{Ba}$  or  $\text{Sr}$ . Upon hole doping, achieved via chemical substitutions, these systems become superconducting with a surprisingly high maximal  $T_c$  of 30 K<sup>4,5,12,13</sup>. As stoichiometry is approached in the pure parent compound, however, the superconductivity gives way to an insulating state featuring a so-called breathing structural distortion, where the  $\text{BiO}_6$  octahedra disproportionate into small and large ones in a rock-salt-like pattern<sup>14-17</sup>.

Although in the early years following the discovery of  $\text{ABiO}_3$ , their breathing distortion was viewed as a result of charge disproportionation of the nominally tetravalent  $\text{Bi}^{4+}$  ions into  $\text{Bi}^{3+}$  and  $\text{Bi}^{5+}$ <sup>18-20</sup>, recent theoretical<sup>21-26</sup> as well as experimental<sup>27-32</sup> studies have seriously challenged this idea. In a more realistic microscopic picture, developed by some of us in Refs. 23,24,26, one starts by recognizing the negative charge-transfer nature of the  $\text{ABiO}_3$  electronic states, *i. e.*, that the  $\text{O}-2p$  states are in fact higher in energy than the semi-core  $\text{Bi}-6s$

states (by amount  $\Delta$ ), as depicted in the top panel of Fig. 1 (a). However, the most important parameter of all shaping the  $\text{ABiO}_3$  electronic structure is the strong hybridization between the  $\text{Bi}-6s$  atomic orbital and the  $a_{1g}$  molecular orbital (MO) formed by the  $\text{O}-2p_\sigma$  orbitals of the oxygen octahedral cage [see Fig. 1 (b)]. It produces a huge splitting between the bonding and anti-bonding bands, much larger than the charge transfer energy, with the latter band landing at the Fermi energy above the  $\text{O}$  non-bonding states, as depicted in the middle panel of Fig. 1 (a). Since the character of the conductance anti-bonding band is predominantly that of the  $\text{O}-a_{1g}$  MO, the average  $\text{Bi}$  oxidation state approaches 3+, leaving two self-doped ligand holes,  $\underline{L}$ , per oxygen octahedron as  $2\text{Bi}^{4+} \rightarrow 2\text{Bi}^{3+}\underline{L}^2$ , in what Alex Zunger and co-workers called a “self-regulating response”<sup>25,33</sup>. Upon the breathing distortion, resulting from the strong electron - breathing phonon interaction, which increases the short-bond length  $\text{Bi}-6s-\text{O}-2p$  hopping integrals and therefore stabilizes further the bonding state, the ligand holes condense pairwise onto the small octahedra as  $2\text{Bi}^{3+}\underline{L}^2 \rightarrow [\text{Bi}^{3+}]_{\text{large}} + [\text{Bi}^{3+}\underline{L}^2]_{\text{small}}$ , resulting in nearly the same valence states for the two inequivalent  $\text{Bi}$  ions<sup>23</sup>, a situation to be called bond, rather than charge, disproportionation. As shown in the bottom panel of Fig. 1 (a), this process is associated with opening of a charge gap at the center of the anti-bonding band of the cubic structure.

With this picture of the  $\text{ABiO}_3$  electronic structure in mind, a further step was taken in Ref. 26 and a general phase diagram was proposed to describe a crossover from a bond- to a charge-disproportionated regime in  $s$ - $p$  cubic perovskites similar to  $\text{ABiO}_3$ . It was shown that there are two main electronic parameters that determine the regime a given system will end up in: the charge-transfer energy  $\Delta$  and the hybridization between the  $B$ -cation  $s$  orbital and the oxygen  $a_{1g}$  MO characterized by the hop-

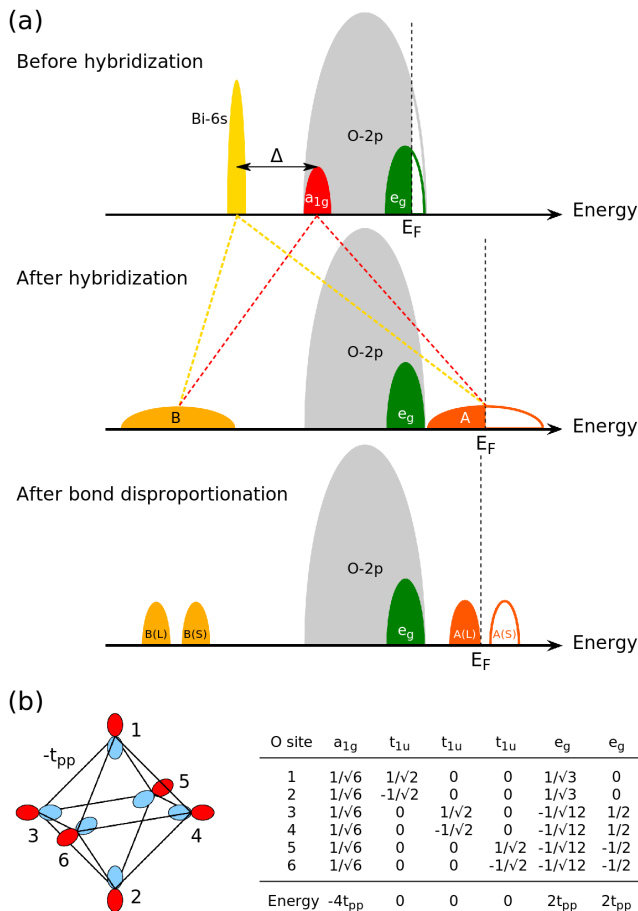


FIG. 1: (a) A schematic diagram of the Bi-6s and O-2p energy levels in  $ABiO_3$  before (top panel) and after (middle panel) hybridization. "A" and "B" denote an anti-bonding and a bonding band, respectively. The bottom panel demonstrates the effect of Bi-O bond disproportionation, whereby the bonding and the anti-bonding bands are each split into two subbands associated with large and small  $BiO_6$  octahedra, denoted as "B(L)", "B(S)", "A(L)", and "A(S)", respectively, and a charge gap is opened as a result. (b) The six O-2p $_{\sigma}$  orbitals of an  $O_6$  octahedron and their molecular orbital combinations,  $a_{1g}$ ,  $t_{1u}$ , and  $e_g$ , with their corresponding energies in units of nearest-neighbor  $pp\sigma$  hopping integral  $-t_{pp}$ .

ping integral  $T_{sp\sigma}$ . However, even though a number of  $s-p$  cubic perovskites other than  $ABiO_3$  are known, such as the recently synthesized  $CsTiCl_3$  and  $CsTiF_3$ <sup>34</sup>, and some of them even superconduct ( $BaPb_{1-x}Sb_xO_3$ <sup>35,36</sup>), no real examples were discussed in Ref. 26 in relation with the proposed phase diagram. In order to fill this gap, in the present paper we use *ab initio* theoretical methods to study the electronic structures of the above mentioned existing  $s-p$  cubic perovskites and also of a systematic series of hypothetical  $ABO_3$  systems, with  $A$  and  $B$  cations being the group IIa and group Va elements, respectively. We hope that this study, conducted in the light of the notion of charge *versus* bond disproportionation, will add to our understanding of superconductivity in the  $s-p$  cubic perovskites and also guide the discovery

TABLE I: GGA equilibrium lattice constants  $a$ ,  $B-s-X-p$  hopping integrals  $t_{sp\sigma}$ , and charge-transfer energies  $\Delta$  of the studied  $ABX_3$  cubic perovskites.

	Has been synthesized?	$a$ (Å)	$t_{sp\sigma}$ (eV)	$\Delta$ (eV)
$MgPO_3$	No	3.667	2.65	1.83
$CaAsO_3$	No	3.919	2.30	-1.44
$SrSbO_3$	No	4.233	2.08	-1.08
$BaSbO_3$	Yes <sup>36</sup>	4.280	2.01	-1.53
$SrBiO_3$	Yes <sup>13</sup>	4.372	1.88	-3.68
$BaBiO_3$	Yes <sup>4</sup>	4.417	1.81	-3.96
$RaMnO_3$	No	4.676	1.46	-8.86
$CsTiF_3$	Yes <sup>34</sup>	4.799	1.24	0.65
$CsTiCl_3$	Yes <sup>34</sup>	5.604	1.16	-0.88

of new superconductors.

## II. METHOD

Our electronic structure calculations are performed within density functional theory (DFT)<sup>37</sup> using the full-potential linearized augmented plane-wave method as implemented in the WIEN2k package<sup>38</sup>. We employ the generalized gradient approximation (GGA)<sup>39</sup> for the exchange-correlation potential. For all our  $s-p$  systems, a simplified cubic  $Pm\bar{3}m$  crystal structure is assumed, with both the tilting and breathing distortions neglected, and the volume is fully relaxed within GGA. The basis set size is fixed by setting  $R_{MT}K_{max} = 7$ , where  $R_{MT}$  is the smallest muffin-tin sphere radius and  $K_{max}$  is the cut-off wave vector. A  $12 \times 12 \times 12$  grid of  $\mathbf{k}$ -points is used for integrating over the first Brillouin zone. Atomic and molecular orbital projections are done within muffin-tin spheres. Projections onto molecular orbitals are done with a modified version of WIEN2k, as discussed in Ref. 40. Tight-binding (TB) parameters are obtained by using the maximally localized Wannier functions (MLWF) method as implemented in the wannier90 code<sup>41</sup>.

## III. RESULTS AND DISCUSSION

Let us first discuss the systematic series of  $ABO_3$   $s-p$  cubic perovskites, where the  $A$  and  $B$  cations are varied down the periodic table as  $MgPO_3$ ,  $CaAsO_3$ ,  $SrSbO_3$ ,  $BaSbO_3$ ,  $SrBiO_3$ ,  $BaBiO_3$ , and  $RaMnO_3$ . Among them, only  $SrBiO_3$ ,  $BaSbO_3$ , and  $BaBiO_3$  exist in nature (see Table I), but our prime interest is to identify general trends in the electronic structure of such  $s-p$  systems.

Figures 2 (a)-(e) and 4 (a)-(e) show the band-structures and the projected densities of states (DOS) of the studied  $ABO_3$  series, respectively. Note that no results for  $SrBiO_3$  and  $BaSbO_3$  are shown as they are very similar to those for, respectively,  $BaBiO_3$  and  $SrSbO_3$ . All the systems demonstrate the same strong bonding-anti-bonding splitting between the  $B-s$  atomic and O- $a_{1g}$  molecular orbitals, with the anti-bonding

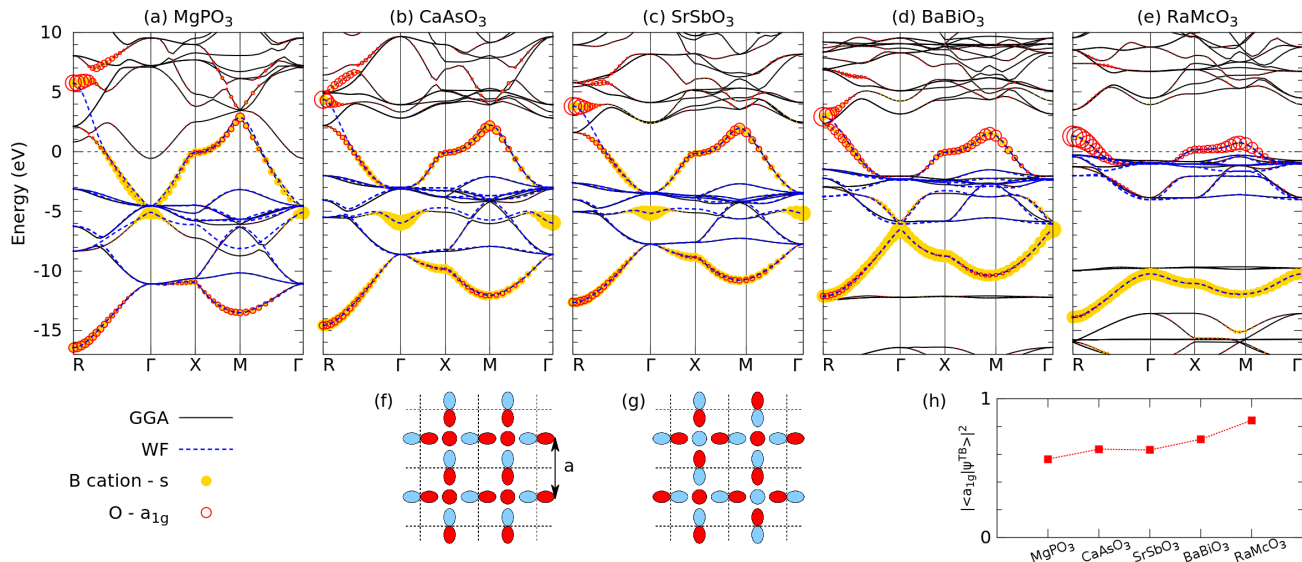


FIG. 2: The electronic band-structures of (a) MgPO<sub>3</sub>, (b) CaAsO<sub>3</sub>, (c) SrSbO<sub>3</sub>, (d) BaBiO<sub>3</sub>, and (e) RaMCo<sub>3</sub> calculated in GGA and plotted with black solid lines. The Fermi energy is set to zero and marked by a horizontal black dashed line. The red and yellow circles indicate the presence of, respectively, the O- $a_{1g}$  and cation  $B-s$  orbital characters in a given Bloch eigenstate, with the amount of their contribution being proportional to the circles' radii. The dashed blue lines represent the eigenstates of the MLWF-based TB model. Panels (f) and (g) use a two-dimensional (2D) analogue of the cubic perovskite structure to explain the absence of hybridization between the O- $2p_{\sigma}$  and  $B-s$  Bloch functions at the  $\Gamma$  point [ $\mathbf{k} = (0, 0, 0)$ ] and its maximum strength at the  $R$  point [ $\mathbf{k} = (\pi, \pi, \pi)$ ], respectively. The dashed lines mark boundaries between 2D unit cells with the lattice constant  $a$ . (h) The amount of the O- $a_{1g}$  molecular orbital character in the anti-bonding band of the  $ABO_3$  TB models,  $|\langle a_{1g}(\mathbf{k}) | \psi^{\text{TB}}(\mathbf{k}) \rangle|^2$ , at the  $R$  point as a function of chemical composition.

band landing at the Fermi level and becoming half occupied. Only in MgPO<sub>3</sub>, there is a second band crossing the Fermi level, which is mainly of the Mg- $3s$  orbital character. As a general trend, the overall band width of the  $B-s - O-2p$  states decreases as we go down from MgPO<sub>3</sub> to RaMCo<sub>3</sub>. Indeed, as the lattice constant increases due to the large ionic radii of the  $A$  and  $B$  cations (see Table I), the direct hopping between oxygen orbitals is decreasing, which results in reduction of the oxygen orbitals' band width, and so does the hopping between oxygen orbitals and the  $B$  cation  $s$  orbitals, which results in reduction of the band width of the  $B-s$  and O- $a_{1g}$  hybrid. On one hand, the narrowing of the oxygen band makes it easier to push the  $a_{1g}$  states up and out of the top of the oxygen band. On the other hand, the reduced  $B-s - O-2p_{\sigma}$  hopping integral  $t_{sp\sigma}$  leads to a flattening of the anti-bonding conduction band in BaBiO<sub>3</sub> and, especially, RaMCo<sub>3</sub>. Correspondingly, the density of states at the Fermi level is strongly increased in these two end members of the series, which makes them more strongly driven towards bond disproportionation and other types of structural distortions. Another important trend in the band structures of the  $ABO_3$  series is the gradual change of the dominating character of the anti-bonding conduction band from one of more  $B-s$  atomic orbital to one of more O- $a_{1g}$  MO character. This is illustrated in Fig. 2 (h) showing the amount of the O- $a_{1g}$  MO character in the anti-bonding band of the  $ABO_3$  TB models (which will be discussed in more detail shortly),  $|\langle a_{1g}(\mathbf{k}) | \psi^{\text{TB}}(\mathbf{k}) \rangle|^2$ , at the  $R$  point as a function

of chemical composition.

It is important to note that the bonding-anti-bonding splitting is strongly  $\mathbf{k}$ -vector dependent, due to the changing symmetry of the Bloch functions involved. The splitting vanishes at  $\Gamma$  [ $\mathbf{k} = (0, 0, 0)$ ], because at this point the Bloch wave function has no  $a_{1g}$  molecular orbital component [Fig. 2 (f)]. In contrast, at the  $R$  point [ $\mathbf{k} = (\pi, \pi, \pi)$ ], the Bloch wave function is of a pure  $a_{1g}$  molecular orbital character in the oxygen  $p_{\sigma}$  orbitals' domain [Fig. 2 (g)], and the splitting reaches its maximum.

In accordance with this logic, the band structure plots of Fig. 2 feature no  $a_{1g}$  character in any of the Bloch states at the  $\Gamma$  point. Also, there is only one state with dominating  $B-s$  character at this  $\mathbf{k}$ -vector, which moves to lower energies towards the end of the  $ABO_3$  series, from around -5 eV in MgPO<sub>3</sub> to -10 eV in RaMCo<sub>3</sub>. Along the  $\Gamma - R$  path (and, actually, at any point other than  $\Gamma$ ), the finite  $B-s - O-2p_{\sigma}$  hybridization is expected to make the bonding band disperse downwards and reach a minimum at  $R$ . While this is what we indeed observe in the band structures of BaBiO<sub>3</sub> and RaMCo<sub>3</sub>, the behavior of the bonding band in the band structures of MgPO<sub>3</sub>, CaAsO<sub>3</sub> and SrSbO<sub>3</sub> appears to be more complex. There, the  $B-s$  state at  $\Gamma$  happens to be energetically above the triply degenerate oxygen molecular orbital  $t_{1u}$  states (positioned at around -11 eV in MgPO<sub>3</sub> and -8 eV in CaAsO<sub>3</sub> and SrSbO<sub>3</sub>). Away from  $\Gamma$ , these oxygen bands disperse upwards and get entangled with the bonding band. This is the reason why in MgPO<sub>3</sub>, CaAsO<sub>3</sub> and SrSbO<sub>3</sub> the character of the bonding  $a_{1g}$

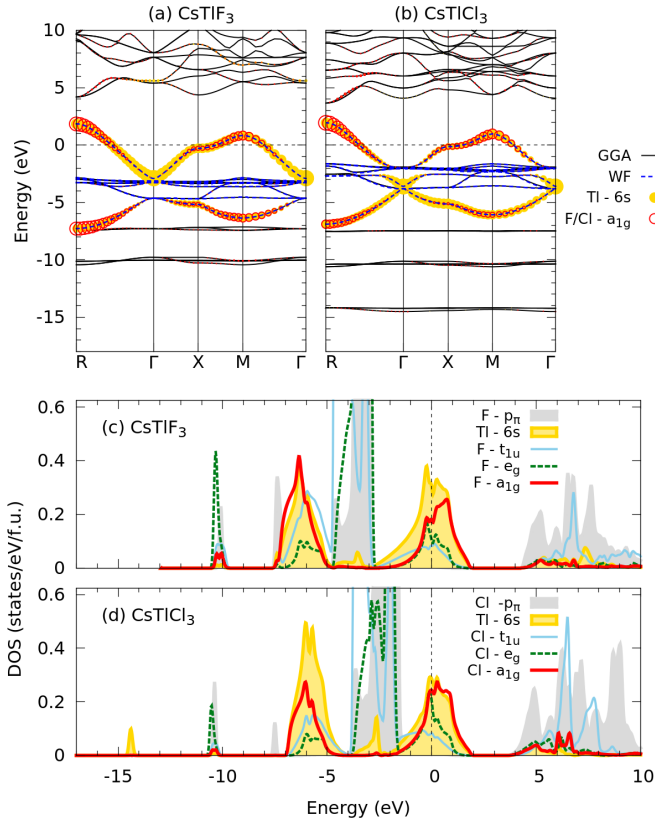


FIG. 3: (a), (b) The electronic band-structures of  $\text{CsTlF}_3$  and  $\text{CsTlCl}_3$ . Notations are similar to those in Fig. 2. (c), (d) Partial densities of states of  $\text{CsTlF}_3$  and  $\text{CsTlCl}_3$ , projected onto the Tl-6s atomic orbital and the molecular combinations of the F- $2p_\sigma$  or Cl- $3p_\sigma$  orbitals. The zero of energy is at the Fermi energy.

and  $B-s$  combination is not continuous.

A similar situation occurs for the anti-bonding band close to the  $R$  point. At this point, in the same three systems, the interatomic orbital hybridizations are strong enough to push the anti-bonding state above the triply degenerate  $B-p$  states and position it at around 4 to 6 eV. Away from  $R$ , the  $B-p$  bands and the anti-bonding band mix with each other, and this is the reason why in these three systems the character of the anti-bonding  $a_{1g}$  and  $B-s$  combination is not continuous either.

Let us now compare our findings about the  $ABO_3$  series with the calculated electronic structures of  $\text{CsTlF}_3$  and  $\text{CsTlCl}_3$ , shown in Fig. 3. These recently synthesized halides<sup>34</sup> also demonstrate the bond disproportionation, and so qualitatively we expect their electronic structure near  $E_F$  to be very similar to the oxides, with O replaced by halogen and the divalent cation with monovalent Cs, also resulting in divalent Tl formally with one electron in a 6s orbital, similar to the tetravalent Bi-based problem. It remains unknown, however, whether hole doping can make the thallium halides superconduct<sup>42</sup>. While we note an overall similarity with the electronic structure of the previously discussed  $ABO_3$  compounds, the Tl-6s – halogen- $a_{1g}$  band splitting is considerably

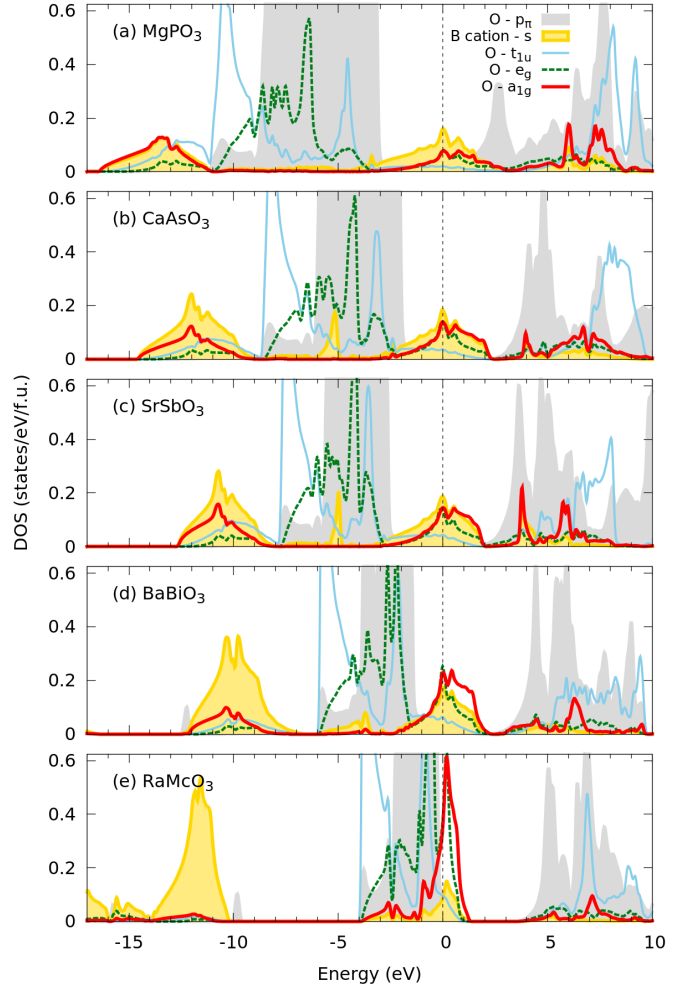


FIG. 4: The partial densities of state projected onto the  $B-s$  atomic orbital and the molecular combinations of  $O-2p_\sigma$  orbitals of (a)  $\text{MgPO}_3$ , (b)  $\text{CaAsO}_3$ , (c)  $\text{SrSbO}_3$ , (d)  $\text{BaBiO}_3$  and (e)  $\text{RaMnO}_3$ . The Fermi energy is set to zero and marked by a vertical black solid line.

smaller. Also, even though the difference between the  $\text{CsTlF}_3$  and  $\text{CsTlCl}_3$  lattice constants is quite significant (Table I), we see only a slight change in the band-widths of their Tl-6s – halogen- $a_{1g}$  band manifolds.

We proceed now to quantifying the observed differences in the electronic structures of the  $ABX_3$  compounds in terms of the  $B-s-X-p$  hybridization strength  $t_{sp\sigma}$  and the charge-transfer energy  $\Delta$ . As was shown in Ref. 26, these are the two main parameters that determine the character of the empty states crossing the Fermi level. We should emphasize that in our convention  $\Delta$  is defined as the difference between the on-site energies of the  $B-s$  atomic orbital and of the  $X-a_{1g}$  MO:  $\Delta = \epsilon(B-s) - \epsilon(X-a_{1g})$ <sup>26</sup>.  $t_{sp\sigma}$  and  $\Delta$  are obtained by calculating MLWF-based TB models for our systems. Similarly to Ref. 24, here we consider 10 orbitals per formula unit: one  $B-s$  and three  $X-p$  orbitals per each of the three anions in a simple cubic unit cell. As one can see in Figs. 2 (a)-(e) and 3 (a)-(b), the resulting TB mod-



els have band dispersions that agree well with the GGA band structures. However, small deviation exists at the  $R$  point of  $\text{MgPO}_3$ ,  $\text{CaAsO}_3$ , and  $\text{SrSbO}_3$ , due to hybridization with higher energy states, as discussed earlier in the paper. We have chosen not to consider the higher energy  $B-p$  orbitals in the TB models because our main focus is on the low-energy scale electron removal and addition states relevant for the physical properties at relatively low temperatures.

The hopping integrals  $t_{sp\sigma}$  are given in Table I. While for the  $ABO_3$  series the value of  $t_{sp\sigma}$  decreases rather monotonically from  $\text{MgPO}_3$  to  $\text{RaMcO}_3$  and is inversely related to the unit cell's size, the  $t_{sp\sigma}$  values of the two halides are surprisingly similar given the big difference between their unit cells' sizes. In order to obtain the charge-transfer energy  $\Delta = \epsilon(B-s) - \epsilon(X-a_{1g})$ , we have applied a basis set transformation from oxygen atomic to oxygen molecular orbitals using the table in Fig. 1 (b). The resulting charge-transfer energy values  $\Delta$  are listed in Table I. In the  $ABO_3$  series,  $\Delta$  varies widely from a positive value of 1.83 eV in  $\text{MgPO}_3$  to a negative value of -8.86 eV in  $\text{RaMcO}_3$ , thus marking a difference between  $\text{MgPO}_3$  and  $\text{CsTiF}_3$ , as being *positive charge-transfer energy* compounds, and the rest of the  $ABO_3$  systems and  $\text{CsTiCl}_3$ , as being *negative charge-transfer energy* compounds. We note again that in all cases, except perhaps  $\text{RaMcO}_3$ , the total bonding-anti-bonding splitting strongly dominates over the charge transfer energy, making the latter less important than the hopping integrals.

The dramatic decrease of  $\Delta$  in the  $ABO_3$  series with  $A$  and  $B$  moving down the periodic table can be understood in terms of relativistic lowering of the  $6s$  and  $7s$  orbital energies in the heavy elements Bi and Mc<sup>43</sup>. In  $\text{RaMcO}_3$ , it takes an extreme form, which, combined with the reduced  $t_{sp\sigma}$  hybridization, results in an almost ionic character of the  $\text{Mc}^{3+}$  ionization state, in agreement with earlier studies<sup>44</sup>. This can be clearly seen from the  $\text{RaMcO}_3$  projected DOS shown in Fig. 4 (e). Similarly to  $\text{Ba}(\text{Sr})\text{BiO}_3$ ,  $\text{RaMcO}_3$  is therefore expected to bond-disproportionate in its ground state as  $2\text{Mc}^{3+}\underline{L}^2 \rightarrow [\text{Mc}^{3+}]_{\text{large}} + [\text{Mc}^{3+}\underline{L}^2]_{\text{small}}$ , with most of the action happening on oxygens. On the other hand, also interesting is the fact that  $\text{BaSbO}_3$  can become superconducting upon substituting Sb with Pb but not with Sn<sup>36</sup>. This again was explained in terms of the relativistic energy lowering of  $\text{Pb-}6s$  states with respect to  $\text{Sn-}5s$  states<sup>35</sup>. The maximal  $T_c$  observed in  $\text{BaPb}_x\text{Sb}_{1-x}\text{O}_3$  is 3.5 K, which is unexpectedly low compared with that of the bismuthates. At this point, we can only speculate that if there is a relation between  $T_c$  and how negative  $\Delta$  is, then optimally hole-doped  $\text{RaMcO}_3$  might have a very high  $T_c$ . Such a relation can be rooted in electron-phonon coupling which might become most efficient in the presence of ligand holes, but of course more theoretical and experimental studies are required to give some validity to this idea. We should also note that the density of states at  $E_F$  is very high in  $\text{RaMcO}_3$  because of the narrowing of the anti-bonding band and this could also support a higher  $T_c$ .

Finally, with the hopping integrals  $t_{sp\sigma}$  and charge-

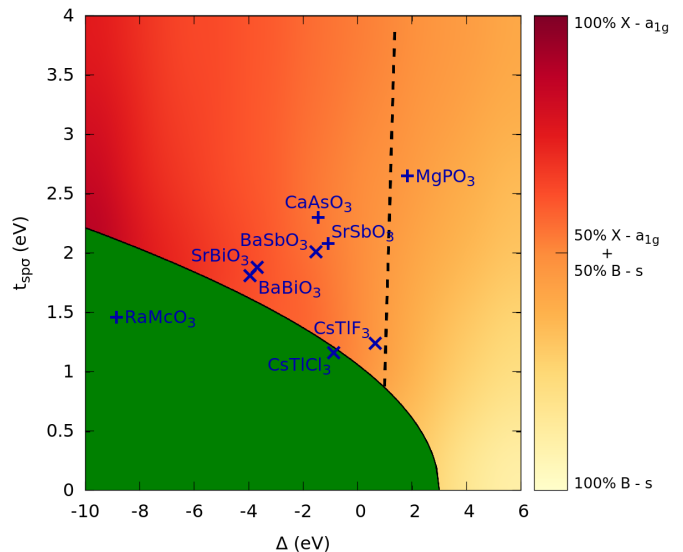


FIG. 5: The phase diagram of Ref. 26 representing the dominant character of holes as a function of the charge-transfer energy  $\Delta$  and hybridization  $t_{sp\sigma}$ . Symbols + and  $\times$  mark the parameters relevant to the hypothetical and existing cubic  $s-p$   $ABX_3$  perovskites, respectively. Green, yellow, and red colors represent the amount of the  $X-e_g$ ,  $X-a_{1g}$ , and  $B$  cation  $s$  orbital contributions to the holes' character, respectively.

transfer energies  $\Delta$  of our studied  $ABX_3$  compounds at hand, we can mark their positions on the phase diagram proposed in Ref. 26. There will be some degree of approximation involved because this phase diagram was obtained for  $\text{BaBiO}_3$  in a bond-disproportionated state using the value of the oxygen band-width  $W$  specific to  $\text{BaBiO}_3$ , but this is not going to obscure observation of general trends that we are most interested in. As explained in Ref. 26, the colors in this phase diagram represent the dominant character of the empty (hole) states above the Fermi level as a function of hybridization and charge-transfer energy. While there is a sharp boundary around the green region where holes reside on  $X-e_g$  orbitals, the  $B-s$  (yellow) and  $X-a_{1g}$  (red) orbitals are always mixed by hybridization and therefore there is a gradual crossover between the yellow and red regions. The black dashed line marks equal contributions from the  $B-s$  and  $X-a_{1g}$  orbitals to the holes' character. Figure 5 is showing now that  $\text{SrBiO}_3$  and  $\text{BaBiO}_3$  are relatively deep in the  $X-a_{1g}$  region, while  $\text{MgPO}_3$ ,  $\text{CaAsO}_3$ ,  $\text{SrSbO}_3$ ,  $\text{BaSbO}_3$ , and  $\text{CsTiF}_3$  are close to having equal  $B-s$  and  $X-a_{1g}$  orbital contributions. As for  $\text{RaMcO}_3$  and  $\text{CsTiCl}_3$ , they land in the  $O-e_g$  region but from their projected DOS [Fig. 4 (e) and Fig. 3 (d)] we know that their hole character is strongly  $O-a_{1g}$ . This discrepancy is due to the mentioned approximations, but it is obvious that  $\text{RaMcO}_3$  must in any case be located very far inside the  $O-a_{1g}$  region close to the  $O-e_g$  border.

#### IV. CONCLUSIONS

In this paper, we have used *ab initio* methods to study the electronic structures of the following  $s$ - $p$  cubic perovskites  $ABX_3$ : the experimentally available  $BaSbO_3$ ,  $SrBiO_3$ ,  $BaBiO_3$ ,  $CsTiF_3$ , and  $CsTiCl_3$ , as well as the hypothetical  $MgPO_3$ ,  $CaAsO_3$ ,  $SrSbO_3$ , and  $RaMcO_3$ . We have used Wannier functions based tight-binding modeling to calculate their hybridization strengths  $t_{sp\sigma}$  between the  $B$ - $s$  and  $X$ - $p$  atomic orbitals and charge-transfer energies  $\Delta$ , which are the two most important parameters that determine the nature of the systems' holes. These calculations have elucidated several trends in  $t_{sp\sigma}$  and  $\Delta$  as one moves across the periodic table, such as the relativistic energy lowering of the  $B$ - $s$  orbital in heavy  $B$  cations leading to strongly negative  $\Delta$  values. Our results have been discussed in connection with the general phase diagram for  $s$ - $p$  cubic perovskites proposed in Ref. 26.

Also, some considerations have been offered regarding a possible relation between the highest achievable superconducting transition temperatures and certain features of the systems' electronic structures, such as the charge-transfer energy  $\Delta$  and the interatomic orbital hybridization  $B$ - $s$  -  $O$ - $2p_\sigma$   $t_{sp\sigma}$ , with the latter primarily controlling the conduction band width and the DOS at the Fermi level. In particular, we observed that the more negative the  $\Delta$  value is the more of the  $X$ - $a_{1g}$  charac-

ter will be there in the valence and conduction bands provided that the hybridization strength is large enough to still push out the  $X$ - $a_{1g}$  bound state. In the case of  $RaMcO_3$  and also  $Ba(Sr)BiO_3$ ,  $\Delta$  is very negative and so the amount of the  $X$ - $a_{1g}$  character in the anti-bonding state will be the largest. As  $\Delta$  becomes even more negative there will be a point where the  $X$ - $a_{1g}$  state no longer is pushed above the  $X$ - $e_g$  state, as illustrated in the phase diagram of Fig. 5. Given the significantly larger maximal  $T_c$  in the hole-doped bismuthates  $Ba(Sr)BiO_3$  than in the hole-doped antimonates  $BaSbO_3$ , superconductivity is apparently enhanced if the charge character of the hole states is mostly  $X$ - $a_{1g}$ , which can possibly be traced down to the enhanced coupling with the breathing mode phonon. However, an even more important feature of the electronic structure that can be responsible for an enhanced  $T_c$  is the increase of the DOS at the Fermi level in  $BaBiO_3$ , due to its reduced  $t_{sp\sigma}$  value. For these reasons, we expect that optimally hole-doped  $RaMcO_3$  might have a very high  $T_c$ .

#### Acknowledgments

This work was supported by Natural Sciences and Engineering Research Council (NSERC) for Canada, CIFAR, and the Max Planck - UBC Stewart Blusson Quantum Matter Institute.

- 
- \* Present affiliation: Department of Physics, Payame Noor University, P.O. Box 19395-3697 Tehran, Iran  
 † foyevtsova@phas.ubc.ca
- <sup>1</sup> Imada et al. Rev. Mod. Phys. **70**, 1039(1998).
  - <sup>2</sup> M. L. Medarde, J. Phys. Condens. Matter **129**, 1679 (1997).
  - <sup>3</sup> J. G. Bednorz and K. A. Muller, Zeitschrift fur Physik B Condensed Matter **64**, 189 (1986).
  - <sup>4</sup> A. W. Sleight, J. L. Gillson, and P. E. Bierstedt, Solid State Commun. **17**, 27 (1975).
  - <sup>5</sup> R. J. Cava, B. Batlogg, J. J. Krajewski, R. Farrow, L. W. Rupp, Jr., A. E. White, K. Short, W. F. Peck, and T. Kometani, Nature **332**, 814 (1988).
  - <sup>6</sup> A. M. Green; A. Ho-Baillie; H. J. Snaith; Nature Photonics, **8(7)**, 506-514 (2014).
  - <sup>7</sup> A. P. Ramirez, J. Phys.: Condens. Matter **9**, 8171(1997).
  - <sup>8</sup> T. Kimura, T. Goto, H. Shintani, K. Ishizaka, T. Arima, Y. Tokura, Nature **426**, 58(2003).
  - <sup>9</sup> H. Jin, S. H. Rhim, J. Im and A. J. Freeman, Scientific Reports **3:1651**, 1(2012).
  - <sup>10</sup> H. Jin, J. Im, and A. J. Freeman, Phys. Rev. B **86**, 121102(R) (2012).
  - <sup>11</sup> B. Yan, M. Jansen and C. Felser, Nature Phys. **9**, 709(2013).
  - <sup>12</sup> L. R. Mattheiss, E. M. Gyorgy, and D. W. Johnson, Phys. Rev. **B37**, 3746 (1988).
  - <sup>13</sup> S. M. Kazakov, C. Chaillout, P. Bordet, J. J. Capponi, M. Nunez-Regueiro, A. Rysak, J. L. Tholence, P. G. Radaelli, S. N. Putilin, and E. V. Antipov, Nature **390**, 148 (1997).
  - <sup>14</sup> D. Cox and A. W. Sleight, Solid State Commun. **19**, 969 (1976).
  - <sup>15</sup> D. E. Cox and A. W. Sleight, Acta Crystallographica Section B **35**, 1 (1979).
  - <sup>16</sup> Q. Zhou, B. J. Kennedy Solid State Commun. **132**, 392(2004).
  - <sup>17</sup> A. Sleight, Physica C **514**, 152 (2015).
  - <sup>18</sup> C. M. Varma, Phys. Rev. Lett. **61**, 2713 (1988).
  - <sup>19</sup> A. Taraphder, H. R. Krishnamurthy, R. Pandit, and T.V. Ramakrishnan, Negative-U Extended Hubbard Model for Doped Barium Bismuthates, Phys. Rev. B **52**, 1368 (1995).
  - <sup>20</sup> I. Hase and T. Yanagisawa, Phys. Rev. B **76**, 174103 (2007).
  - <sup>21</sup> L. F. Mattheiss and D. R. Hamann, Phys. Rev. B **28**, 4227 (1983).
  - <sup>22</sup> W. A. Harrison, Phys. Rev. B **74**, 245128 (2006).
  - <sup>23</sup> K. Foyevtsova, A. Khazraie, I. Elfimov and G. Sawatzky, Phys. Rev. B **91**, 121114(R) (2015).
  - <sup>24</sup> A. Khazraie, K. Foyevtsova, I. Elfimov, and G. A. Sawatzky, Phys. Rev. B **97**, 075103 (2018).
  - <sup>25</sup> G. M. Dalpian, Q. Liu, J. Varignon, M. Bibes, and Alex Zunger, Phys. Rev. B **98**, 075135 (2018).
  - <sup>26</sup> A. Khazraie, K. Foyevtsova, I. Elfimov, and G. A. Sawatzky, Phys. Rev. B **98**, 205104 (2018).
  - <sup>27</sup> J. de Hair and G. Blasse, Solid State Commun. **12**, 727 (1973).
  - <sup>28</sup> A. F. Orchard and G. Thornton, J. Chem. Soc. Dalton Trans., 1238 (1977).
  - <sup>29</sup> G. K. Wertheim, J. P. Remeika, and D. N. E. Buchanan, Phys. Rev. B **26**, 2120 (1982).
  - <sup>30</sup> S. Salem-Sugui, Jr., E. E. Alp, S. M. Mini, M. Ramanathan, J. C. Campuzano, G. Jennings, M. Faiz, S. Pei, B. Dabrowski, Y. Zheng, D. R. Richards, and D. G. Hinks,

- Phys. Rev. B **43**, 5511-5515(1991).
- <sup>31</sup> N. C. Plumb, D. J. Gawryluk, Y. Wang, Z. Ristic, J. Park, B. Q. Lv, Z. Wang, C. E. Matt, N. Xu, T. Shang, K. Conder, J. Mesot, S. Johnston, M. Shi, and M. Radovic, Phys. Rev. Lett. **117**, 037002 (2016).
- <sup>32</sup> S. Balandeh, R. J. Green, K. Foyevtsova, S. Chi, O. Foyevtsov, F. Li, and G. A. Sawatzky, Phys. Rev. B **96**, 165127 (2017).
- <sup>33</sup> H. Raebiger, S. Lany, and A. Zunger, Charge self-regulation upon changing the oxidation state of transition metals in insulators. Nature **453**, 763-766 (2008).
- <sup>34</sup> M. Retuerto et al., Chem. Mater. **25**, 4079 (2013).
- <sup>35</sup> D. J. Singh, D. A. Papaconstantopoulos, J. P. Julien, F. Cyrot-Lackmann, Phys. Rev. B **44**, 9519(1991).
- <sup>36</sup> R. J. Cava et al., Nature **339**, 293 (1989).
- <sup>37</sup> W. Kohn, L.J. Sham, Phys. Rev. **140**, A1133(1965).
- <sup>38</sup> P. Blaha, K. Schwarz, G. K. H. Madsen, D. Kvasnicka, and J. Luitz, WIEN2K, An Augmented Plane Wave + Local Orbitals Program for Calculating Crystal Properties (Karlheinz Schwarz, Techn. Universit?at Wien, Austria, 2001).
- <sup>39</sup> J.P. Perdew, K. Burke, M. Ernzerhof, Phys. Rev. Lett. **77**, 3865(1996).
- <sup>40</sup> K. Foyevtsova and G. A. Sawatzky, Journal of Modern Physics **10**, 953-965 (2019).
- <sup>41</sup> A. A. Mostofi, J. R. Yates, Y.-S. Lee, I. Souza, D. Vanderbilt, and N. Marzari, Computer Physics Commun. **178**, 685 (2008).
- <sup>42</sup> M. Retuerto et al., Inorg. Chem. **54**, 1066-1075 (2015).
- <sup>43</sup> P. Pykko, Chem. Rev. **88**, 563 (1988).
- <sup>44</sup> O. L. Keller Jr., C. W. Nestor Jr., and Burkhard Fricke. J. Phys. Chem., **78(19)**, 1949 (1974).